Current Research in Microbial Sciences 7 (2024) 100309

Contents lists available at ScienceDirect

Current Research in Microbial Sciences

journal homepage: www.sciencedirect.com/journal/current-research-in-microbial-sciences

Differential gliding motility responses of *Chryseobacterium* sp. strain PMSZPI isolated from uranium ore deposit on hard and soft substrates

Lalitharashmi Yermunja [a,b], Celin Acharya [a,b,*]

[a] *Molecular Biology Division, Bhabha Atomic Research Centre, Trombay, Mumbai, 400085, India*
[b] *Homi Bhabha National Institute, Anushakti Nagar, Mumbai, 400094, India*

ARTICLE INFO

Keywords:
Gliding motility
Chryseobacterium
Soft and hard agar
Spreading and non-spreading
Gene expression

ABSTRACT

The *Bacteroidota* bacterium, *Chryseobacterium* sp. strain PMSZPI isolated from sub-surface soil of uranium ore deposit was shown to move on solid surfaces via gliding motility resulting in the formation of thin spreading colonies. In this study, we attempted to understand the influence of the surfaces, soft or hard/rigid, on the motility behaviour of PMSZPI cells. The computational tool T9GPred in combination with LC-MS/MS analysis established the presence of orthologs of vital gliding motility proteins in PMSZPI. We analyzed the single cell or population motility phenotypes of PMSZPI under spreading and non-spreading conditions. A low percentage of agar or soft agar (0.35 %) with low nutrient levels induced more active gliding motility in individual cells leading to increased colony spreading. Microscopic analyses indicated the self-assembly of the gliding cells into irregular edged or spherical microcolonies based on the agar concentration. Cells moved at a speed of 0.6 μm s^{-1} on low-percentage gliding permissive agar (0.35 %) surface in contrast to significant inhibition of motility on rigid or hard agar (1.5 %) surface. RNA sequencing and real-time quantitative PCR (qPCR) analysis revealed increased expression of gliding motility genes under low agar conditions consistent with increased spreading behaviour. These findings provide the first glimpse into the gliding motility behaviour of a *Bacteroidota* bacterium from metal enriched environment that apparently could have implications on bacterial adaptation to changing surface environments.

1. Introduction

Bacteria move and relocate in different ways, facilitating their survival in biotic and abiotic environments. Bacterial motility helps with nutrition detection in the surroundings or escaping from predation or any other stressful factors and stimulates bacterial multifaceted social behaviour. Different forms of bacterial motility have evolved with each form displaying diverse abilities for enabling the survival of the organism with a particular lifestyle or in a specific environment. Bacteria belonging to the *Bacteroidota* phylum move over solid surfaces in the absence of extracellular motility appendages in a process termed gliding motility (McBride 2019). Unlike the other types of bacterial motility mechanisms such as swimming, swarming and twitching motility which are aided by locomotory apparatus like type IV pili or flagella, gliding motility in *Bacteroidota* is appendage-free motion driven by Gld and Spr proteins (McBride 2019; Sato et al., 2010). These proteins are components of the novel macromolecular membrane-bound protein transport machinery known as the Type IX secretion system (T9SS) (Chang et al., 1984; McBride 2019). *Porphyromonas gingivalis,* a human non-motile periodontal pathogen and *Flavobacterium johnsoniae*, a motile free-living organism have been extensively studied for T9SS. The T9SS in *P. gingivalis* comprises several proteins including PorK, PorL, PorM, PorN, Sov, PorW, PorT, PorP, PorV and PG1058 (McBride 2019; Sato et al., 2010). The orthologs of the first seven proteins stated for T9SS in *P. gingivalis* are GldK, GldL, GldM, GldN, SprA, Spr E and SprT in *F. johnsoniae* that constitute the mandatory components of T9SS and are required for gliding motility and protein secretion (McBride 2019). Other than these proteins, Gld B, Gld D, Gld H and Gld J are also part of the T9SS, which are essential for gliding motility in *F. johnsoniae* (Braun et al., 2005; Braun and McBride 2005; Shrivastava et al., 2013; Sato et al., 2010). The absence of any single protein from the aforementioned obligatory gliding motility proteins confers non-motility in *Bacteroidota* members that was observed in *P. gingivalis* as evolutionarily it lacked GldB, GldD, GldH and GldJ (Sato et al., 2010; McBride 2019). Hence, the two systems- gliding motility and T9SS are interwoven and the multi-protein complex assembly is necessary for the functioning of the motility

* Corresponding author at: Molecular Biology Division, Bhabha Atomic Research Centre, Trombay, Mumbai 400 085, India.
E-mail address: celin@barc.gov.in (C. Acharya).

https://doi.org/10.1016/j.crmicr.2024.100309

Available online 6 November 2024

machinery.

Despite decades of research, dedicated gliding motility functionalities have not been elucidated and characterized in detail in any motile *Bacteroidota* member other than *F. johnsoniae*. In this study, we attempted to unveil the gliding motility characteristics of a *Bacteroidota,* soil-dwelling bacterium, *Chryseobacterium* sp. strain PMSZPI isolated from the sub-surface soil of uranium ore deposit in Domiasiat in Meghalaya, India (Kumar et al., 2013). The organism lacked locomotory organelles and moved over the solid surfaces by gliding motility possibly powered by T9SS (Khare et al., 2020; 2022a). The genome sequence of PMSZPI revealed the presence of 11 orthologous genes mandatorily required for gliding motility in *F. johnsoniae - gldB, gldD, gldH, gldJ, gldK, gldL, gldM, gldN, sprA, sprE,* and *sprT*. The core set of gliding motility genes in PMSZPI included the central components of the T9SS (Khare et al., 2020, 2022a). The organism exhibited functional gliding motility on nutrient-deficient soft agar plates resulting in thin spreading colonies with irregular terraced edges (Khare et al., 2022a). In this study, we used *Chryseobacterium* sp. strain PMSZPI as a model system to interrogate how the surface environment affected the motility of PMSZPI cells leading to spreading or non-spreading colony formation. We performed the proteomic analysis of the membrane fraction of PMSZPI cells for the identification of gliding motility proteins. We further investigated the collective movement of PMSZPI cells that self-assembled into the microcolonies and tracked the trajectory of individual gliding cells for the assessment of the gliding speed of the cells. The overall transcriptional responses of PMSZPI cells under spreading and non-spreading conditions on soft and hard agar surfaces respectively with special emphasis on T9SS-associated gliding motility genes were established. Our findings provide insights into gliding motility behaviour on various surfaces in the environmental bacterium, *Chryseobacterium* sp. strain PMSZPI which suggested towards its adaptation to a low nutrient, metal enriched environment typical of its isolation site of the uranium ore deposit. It is the first study that details the gliding motility responses in an environmental bacterium isolated from a uranium/heavy metal augmented habitat.

2. Materials and methods

2.1. Bacterial strain and culture conditions

Chryseobacterium sp. strain PMSZPI was isolated previously from the sub-surface soil of the uranium ore deposit of Domiasiat in Meghalaya, India (Kumar et al., 2013). The pre-culture of PMSZPI was initiated by streaking frozen 25 % glycerol cell stock onto Luria-Bertani (LB) agar plates that were incubated overnight at 30 °C. The isolated colony from the plate was inoculated into 10 ml of Luria-Bertani (LB) medium and incubated overnight under shaking (120 rpm) at 30 °C. Overnight-grown cultures were then inoculated into LB medium to initiate the experiments.

2.2. Sequence analysis of core T9SS linked gliding motility proteins

Different draft and complete genome sequences of twenty-five organisms belonging to the phylum *Bacteroidota* were analyzed in this study to examine the relationship of the orthologs of T9SS linked gliding motility proteins- GldK, GldL, GldM, GldN, GldB, GldD, GldH, GldJ, SprA, SprE and SprT. The analysis included representative organisms of each class of *Bacteroidota* including (i) *Porphyromonas gingivalis* ATCC 33,277, *Prevotella intermedia* ATCC 25,611, *Marinilabilia salmonicolor* JCM 21,150, *Barnesiella viscericola* C46, DSM 18,177, *Alkaliflexus imshenetskii* Z-7010, DSM 15,055 of class *Bacteroidia*, (ii) *Gramella forsetii* KT0803, *Capnocytophaga ochracea* VPI 2845, DSM 7271, *Flavobacterium johnsoniae* UW101, ATCC 17,061, *Cellulophaga lytica* LIM-21, DSM 7489, *Riemerella anatipestifer* A350/72, DSM 15,868, *Flavobacterium columnare* ATCC 49,512, *Gramella echinicola* DSM 19,838, *Algibacter lectus* DSM 15,365, *Aquimarina longa* SW024, *Schleiferia thermophila* DSM 21,410, *Arenibacter algicola* SMS7, *Chryseobacterium* sp. PMSZPI, *Flavobacterium psychrophilum* OSU THCO2–90 of class *Flavobacteria*, (iii) *Flexibacter flexilis* DSM 6793, *Cytophaga hutchinsonii* ATCC 33,406 of class *Cytophagia*, (iv) *Saprospira grandis Lewin* of class *Saprospria,* (v) *Chitinophaga pinensis* UQM 2034, DSM 2588 of Class *Chitinophaga* and (vi) *Pedobacter heparinus* HIM 762–3, DSM 2366, *Sphingobacterium wenxiniae* DSM 22,789 of class *Sphingobacterium*. The Integrated Microbial Genomes (IMG version 3.5) website at http://img.jgi.doe.gov/ was used to acquire the genomes of these organisms. Homology analysis was conducted with the IMG Gene BLAST tool by using gliding motility and T9SS genes of *F. johnsoniae* as reference (E values were set at 1e-5). The resultant sequences were used to create a maximum likelihood tree using MEGA 11 (Tamura et al., 2021). The ClustalW analysis was used for multiple sequence alignment of gliding and T9SS protein sequences. The models predicted by MEGA 11 were analyzed and the model with the lowest BIC score (Bayesian Information Criterion) was used to generate a Maximum likelihood (ML) phylogenetic tree for the aligned sequences. The consistency of individual trees was confirmed with bootstrap replications of 500–1000.

2.3. Prediction of Chryseobacterium PMSZPI specific T9SS-gliding motility proteins

The protein sequences of PMSZPI were downloaded in fasta format from the NCBI database (txid1033900). The fasta file was then uploaded to the T9GPred web interface (https://cb.imsc.res.in/t9gpred/) (Sahoo et al., 2023) for the prediction of the presence and annotation of T9SS and gliding motility-specific proteins.

2.4. Liquid chromatography-tandem mass spectrometry (LC-MS/MS) analyses of T9SS-gliding motility proteins

Chryseobacterium sp. PMSZPI cultured on 1/10 LB medium was incubated at 30 °C for 24 h and was processed for preparation of the membrane fraction. The culture was centrifuged at 16,000x*g* for 10 min, and the resulting cell pellet was washed thrice with wash buffer (50 mM Tris–HCl+1 mM $CaCl_2$ + 0.02 % NaN_3) and resuspended in the same buffer for sonication. The lysed culture was centrifuged at 30,000 x *g* for 20 min. The resulting pellet containing the membrane fraction was dissolved in 10 mM NH_4HCO_3 (pH 8) with 5 % SDS. The quality of the proteins in the membrane fraction was assessed by resolving them on 15 % SDS-PAGE analysis followed by Coomassie Brilliant Blue staining. For LC-MS/MS analysis, the membrane fraction was digested and reduced with 5 mM TCEP (Singh et al., 2022). The sample was then alkylated with 50 mM iodoacetamide and digested with Trypsin (1:50, Trypsin/lysate ratio) for 16 h at 37 °C. The digests were cleaned using a C18 silica cartridge to remove the salt and dried using a speed vac. The dried pellet was resuspended in buffer A (2 % acetonitrile, 0.1 % formic acid). Experiments were performed on an Easy-nLC-1000 system coupled with an Orbitrap Exploris mass spectrometer, Thermo Scientific. Peptide sample (1μg) was loaded on C18 column 15 cm, 3.0 μm Acclaim PepMap (Thermo Fisher Scientific) and separated with a 0–40 % gradient of buffer B (80 % acetonitrile, 0.1 % formic acid) at a flow rate of 300 nl/min and injected for MS analysis. LC gradients were run for 110 min. MS1 spectra were acquired in the Orbitrap (Max IT = 60 ms, AGQ target = 300 %; RF Lens = 70 %; R = 60 K, mass range = 375−1500; Profile data) (Singh et al., 2022). Dynamic exclusion was employed for 30 s excluding all charge states for a given precursor. MS2 (Max IT= 60 ms, R = 15 K, AGC target 100 %) spectra were collected for the top 20 peptides. All samples were processed and the RAW files generated were analyzed with Proteome Discoverer (v2.5) against the *Chryseobacterium* Uniprot database. For dual SEQUEST and Amanda search, the precursor and fragment mass tolerances were set at 10 ppm and 0.02 Da, respectively. The protease used to generate peptides, i.e., enzyme specificity was set for trypsin/P (cleavage at the C terminus of "K/R: unless followed by "P"). Carbamidomethyl on cysteine as fixed modification and

oxidation of methionine and N-terminal acetylation were considered as variable modifications for database search. Both peptide spectrum match and protein false discovery rate were set to 0.01 FDR. Three biological replicates were used for the analysis. The resultant MS/MS data was assessed using SEQUEST and Amanda search engines based on the UniProt database. Subsequently, the sequences of identified proteins were searched using BLAST to detect homologous sequences in PMSZPI.

2.5. Gliding motility and structural analysis of colonies

For gliding motility assays, the cells were grown overnight in LB broth at 30 °C with shaking (120 rpm). The cultures were harvested by centrifugation at 6000 x *g* for 3 min and were adjusted to an $OD_{600\ nm}$ 1.0 with fresh LB and 10 μl of the resulting cell suspension were spotted on to the centre of 1/10 LB with agar concentration ranging from 0.35 % to 1.5 % in petri plates (9 cm in diameter). These plates were then incubated at 30 °C for 24 h Following incubation, the plates were visualized and imaged under white light using the SynGene: GBox (Cambridge, UK) gel documentation system. The colony sizes were calculated from images using ImageJ.

For stereomicroscopy, the overnight cultures of PMSZPI in LB medium were adjusted to $OD_{600\ nm}$ 1.0 and 10 μl from the resulting cell suspension were spotted onto the centre of 1/10 LB agar medium with agar concentration of 0.35 % and 1.5 % in petri plates. The non-spreading and spreading microcolonies post 24 h of incubation were further observed under a stereomicroscope (Olympus SZX7, Japan) and photographed using a Sony DSCWX500 camera.

The structural analysis of the edges of the spreading and non-spreading colonies was evaluated using bright field (BF) microscopy that was subsequently correlated with scanning electron microscopy (SEM) using a correlative slide holder (Khare et al., 2022b). For this, the coverslips were gently placed on the edges of the microcolonies and thereafter these coverslips carrying the impressions of colony edges were picked up with forceps. The coverslips were then fixed with 2.5 % glutaraldehyde and were serially dehydrated in 20, 30, 50, 70, 90, and 100 % ethanol, before being sputter coated with gold. The coverslips were placed onto the correlative slide holder and then subjected to BF imaging (Zeiss Axio Imager Z2, UK). A three-point calibration was performed semi-automatically with the AxioVision Shuttle and Find software module, after which the bright-field (BF) images of the colony edges were captured using the Zeiss Axio Imager Z2 and the EC Plan-Neofluar 10× (NA. 0.3, DIC I) objective, along with the Zeiss Axiocam 503 mono camera (Khare et al., 2022b). The region of interest on the colony edges was defined in the BF images using the Shuttle and Find software module, to further investigate with SEM. The correlative slide holder was then transferred to the motorized stage of SEM (EVO 18 Research, Carl Zeiss, UK) and the coordinate system of the slide holder was recalibrated (Khare et al., 2022b). The BF digital images of the colony edges were loaded onto the Shuttle and Find module to retrieve the selected areas in SEM and were correlated. The correlated sites were further imaged using SEM at higher magnification for better morphological details of the colony edges.

Live-dead staining of cells in spreading and non-spreading colonies was performed in accordance with the Live/Dead BacLight Viability kit (Molecular Probes) protocol. The impressions of the cells from the centre and periphery of spreading colonies were taken on clean coverslips. Cells from non-spreading microcolonies were sampled using a nichrome wire loop and suspended in water. We did not use a nichrome loop for collecting cells from spreading colonies because of the soft or semi-solid agar. The cells from non-spreading colonies were subjected to centrifugation. Equal volumes of Syto9 and PI from the kit, at concentrations of 5 μM and 30 μM respectively, were combined and were used to stain the cells. These were then incubated in the dark at room temperature for 15 min, following which they were washed with water. The cultures were mounted on a clean glass slide, covered with a glass coverslip and a drop of lens oil for imaging using a fluorescence microscope (Leica, DM 3000 LED, Germany) with an excitation-emission maximum of Syto9 and PI at 483- 503 nm and 535- 615 nm respectively.

2.6. Individual and cooperative cell motility

To track the motility of the individual cells, overnight grown PMSZPI cultures were adjusted to $OD_{600\ nm}$ 0.1 with LB and 1 μl of the suspension was placed on a clean glass slide covered with a thin layer of 1/10 LB with 0.35 % or 1.5 % agar medium and incubated at 30ºC for 3 h in moist chamber. The slides were then subjected to bright field microscopy (Carl Zeiss Axioscop 40 microscope with a charge-coupled device CCD Axiocam MR Zeiss camera). A total of 12 microscopic fields containing sparsely spread cells were subjected to time lapse video microscopy (25 frames per second). The frames were processed on ImageJ for mask generation. Further, *z*-projections were generated and were used to create the kymographs. The generated kymographs were manually traced with the line segment tool to calculate the mean speed of individual PMSZPI cells using the velocity tool plugin.

For cooperative cell motility, overnight grown PMSZPI cultures were adjusted to $OD_{600\ nm}$ 1.0 with LB, and 1 μl of the suspension was placed on a thin layer of 1/10 LB with 0.35 % or 1.5 % agar medium on a clean glass slide. The advancing edges of the colony were viewed under BF microscope (Carl Zeiss Axioscop 40 microscope with a charge-coupled device CCD Axiocam MR Zeiss camera) to capture time-lapse images post 3 h of incubation at 30 °C. The recorded images for every 2 min were analyzed for percentage coverage of progressing colony edges using ImageJ.

These colonies were further incubated at 30 °C for 24 h and visualized with bright field microscope (Carl Zeiss Axioscop 40 microscope with a charge-coupled device CCD Axiocam MR Zeiss camera) for *z*-stacking. The images of edges and centers of spreading (11 and 15 slices respectively) and non-spreading colonies (15 and 74 slices respectively) were recorded for colony thickness measurement.

2.7. RNA sequencing and differential gene expression analysis

RNA was isolated from spreading and non-spreading PMSZPI colonies on 1/10 LB medium with 0.35 % and 1.5 % agar respectively. PMSZPI cells were grown overnight in LB broth at 30 °C with shaking (120 rpm). The cultures were harvested by centrifugation at 6000 x *g* for 3 min and were adjusted to an OD_{600nm}1.0 with fresh LB. The resulting cell suspension (10 μl) was spotted onto the centre of 1/10 LB 0.35 % or 1/10 LB 1.5 % agar medium in petri plates (9 cm in diameter) and incubated at 30 °C for 24 h The cultures from the spreading and non-spreading colonies were suspended in DEPC-treated MilliQ water and used for RNA isolation. The suspensions were centrifuged for 20 min at 10,000 x *g* and washed to remove the traces of agar media. The resulting cell pellets were resuspended in trizol reagent and incubated at 20 °C for 30 min. The contents were then thawed on ice to which 100 μl of 1-bromo-3-chloropropane was added and the resulting solutions were centrifuged at 4 °C for 20 min at 10,000 x *g*. The clear supernatant was aliquoted into fresh tubes and 600 μl of isopropyl alcohol was added and centrifuged. The RNA thus obtained was washed thrice with 70 % ethanol and dried under laminar airflow. RNA quality was checked by visualizing 16S and 23S rRNA bands on 1 % agarose gel. RNA concentrations ($OD_{260\ nm}$) and purity ($OD_{260/280}$) were determined by a microplate reader (Biotek, Germany). DNA contamination was checked ahead of cDNA preparation. Three technical replicates post 24 h of incubation at 30 °C were reverse transcribed to cDNA and sequenced using Illumina HiSeq 4000/ NovaSeq 6000. The raw reads were filtered using Trimmomatic for quality scores and adapters. Filtered reads were aligned to HISAT2 to quantify reads mapped to each transcript. A total number of uniquely mapped reads was counted using feature counts. The uniquely mapped reads were then subjected to differential gene expression using DeSeq2.

2.8. Reverse transcriptase quantitative PCR (RT-qPCR) analysis

RNA was extracted from spreading and non-spreading colonies. The extracted RNA was then used to generate cDNA using ReadyScript™ cDNA Synthesis Mix from Sigma, following the manufacturer's instructions. RT-PCR was performed on the Rotor-Gene 5plex HRM platform, Qiagen (Netherlands) to evaluate the differential expression of the core T9SS and gliding motility genes (*gldK, gldL, gldM, gldN, gldB, gldD, gldH, gldJ, sprE, and sprT)*. The 16S rRNA gene was used as the reference gene. The Ct values of the test genes were normalized with Ct values of 16S rRNA gene for fold change calculations. The primers used for this study are listed in Table 1.

2.9. Statistical analysis

The sizes of the spreading colonies were measured from technical triplicate plates for the three independent biological experiments performed. The values are represented as the mean ± SEM. The cell speeds of ~50 cells are represented ± SEM on dot plot. qRT-PCR are represented as the mean ± SEM of three independent biological experimental measurements. The statistical analyses and graphs were plotted using GraphPad Prism 8.0.2 (GraphPad Software, San Diego, California USA).

2.10. Data deposition

The RNA sequencing data reported in this study is deposited in the form of raw sequencing reads in sequence archive reads database (https://www.ncbi.nlm.nih.gov/sra) under accession number PRJNA1138896.

3. Results

3.1. Phylogenetic relationship of core T9SS-gliding motility proteins amongst the Bacteroidota members

Phylum *Bacteroidota* includes a wide range of diverse microorganisms that are known to harbour T9SS genes. A subset of gliding motility proteins comprises T9SS, the presence of which confers the motility among the *Bacteroidota* members (McBride 2019). The phylogenetic relationship of the orthologs of essential T9SS-gliding motility proteins - GldK, GldL, GldM, GldN, SprA, SprE, SprT, GldB, GldD, GldH, and GldJ, among the *Bacteroidota* members was studied. Due to incomplete annotation of genes in PMSZPI, the protein sequences of *F. johsoniae* were used as queries in IMG to perform the BLASTP analysis for 25 different members of *Bacteroidota*. Analysis of the orthologous gliding motility proteins revealed the closest relationship of PMSZPI with *Riemerella anatipestifer* (Fig. S1). The gliding motility machinery has been extensively studied in *F. johnsoniae* but it was found to be distantly related to *Chryseobacterium* PMSZPI (Fig. S1). BLASTP analysis of the gliding motility proteins between the two organisms, *Chryseobacterium* PMSZPI and *Riemerella anatipestifer* showed ~ 70 % identity indicating the similarity of proteins between the organisms belonging to the same family, Weeksellaceae (Table S1). On the contrary, the percentage identity of PMSZPI gliding proteins with *F. johnsoniae* ranged around 30 %−50 % (Table S1).

Table 1
List of primers used for RT-PCR.

Primer	Sequence
GldKF	5`ATTGTCTGCGTCAGTAGCAT 3`
GldKR	5` CTGCTTCATCCATGAAGA 3`
GldLF	5` CGGTAATATGGCTCTTACTGT 3`
GldLR	5` TCAGCAAATTGAGCGCCTGTA 3`
GldMF	5` CTCGTCAGAAGATGATCAACCT 3`
GldMR	5` CCGGAACCTGTTGAGCTTTAGC 3`
GldNF	5` CCCAGACTATTCTGAATGCTTCT 3`
GldNR	5` CCATCCGGATTATCGTAATA 3`
GldBF	5` CGGTTTCATGGGAGATGGCA 3`
GldBR	5` CCGGTAAAAACGCATCCTGT 3`
GldDF	5` CCTTACGGAGAACTGCGTCT 3`
GldDR	5` TCTGCTTCTTTGATGTGCTCAG 3`
GldHF	5` TTGAGCTGTAACTCTTCTCCTGG 3`
GldHR	5` TCTTATTCTGGAGATTGGTGAAGTT 3`
GldJF	5` TCAGGAACCAGCAAAGGTGG 3`
GldJR	5` TGCGAGGCGTGTTATTCCAA 3`
SprEF	5` GGAAGTGATCTTGGCCAGTCAACTG 3`
SprER	5` CCGAATACTTATTGATCGCT 3`
SprTF	5` ACGCGCAATTTAGAACCCG 3`
SprTR	5` CCAAATAATCATTCAGTCTCCATT 3`

3.2. T9GPred web tool predicts Chryseobacterium PMSZPI specific T9SS linked gliding motility proteins

The T9SS is amongst the least characterized secretion systems in the bacteria and is known to transport proteins across the outer membrane (OM) exclusively in the *Bacteroidota* members. The web-based tools exclusively for the prediction of T9SS effector proteins as well as presence or absence of T9SS-associated gliding motility in bacterial genomes are lacking. A dedicated computational tool, T9GPred, was developed for the prediction of T9SS as well as T9SS-associated gliding motility and secreted proteins in the *Bacteroidota* phylum (Sahoo et al., 2023). In this study, we used T9GPred for prediction of the putative T9SS and gliding motility proteins in *Chryseobacterium* sp. PMSZPI (Table 2). The tool precisely predicted the presence of (a) the core gliding-T9SS proteins from the draft genome of PMSZPI (Table 2) and (b) T9SS-associated gliding motility (Fig. S2). The versatile Hidden Markov Model (HMM) protein profiling used in this prediction tool accurately identified the T9SS-associated proteins thus assisting in precise annotations. Additionally, it detected certain other gliding-T9SS-associated proteins including PorQ, PorU and FtsX. The predicted PorQ and PorU have been annotated as penicillin-binding proteins and hypothetical proteins, respectively, in the PMSZPI genome deposited at NCBI (Khare et al., 2020). Overall, T9GPred identified the occurrence of the T9SS secretory system and gliding motility in PMSZPI. The proteins other than those associated with gliding motility and secreted by T9SS have not been included here in this study.

3.3. Identification of T9SS linked gliding motility proteins in PMSZPI

Analysis of triplicate membrane fractions of PMSZPI by LC-MS/MS resulted in the identification of all the core gliding motility components in *Bacteroidota*- GldK, GldL, GldM, GldN, GldB, GldD, GldH, GldJ, SprA, SprE and SprT (Table 3). The experimental evidence for the expression of gliding motility proteins was obtained by the proteomic analysis in this study that was earlier observed in the genome analysis of

Table 2
Proteins associated with T9SS and gliding motility in PMSZPI predicted using T9GPred.

Protein	GenBank ID
SprA	PKF72459.1
PorQ	PKF75956.1
GldJ	PKF74014.1
GldN	PKF73704.1
GldL	PKF73706.1
FtsX	PKF73293.1
PorU	PKF74013.1
GldH	PKF75271.1
GldK	PKF73707.1
GldD	PKF74924.1
GldA	PKF73961.1
GldB	PKF74149.1
GldM	PKF73705.1
SprE	PKF75138.1
SprT	PKF73553.1

Table 3
LC-MS/MS analysis of T9SS-gliding motility proteins in the membrane fraction of PMSZPI.

Accession	Description	Coverage[%]	# AAs	MW[kDa]
A0A2N0XCN5	GldM	65	529	58.2
A0A2N0XCS4	GldL	60	230	25.9
A0A2N0XCY5	GldN	57	270	32.2
A0A2N0XE64	GldB	54	328	38.1
A0A2N0XCT4	GldK	53	473	53.3
A0A2N0XDK2	GldJ	42	533	61.2
A0A2N0XH82	GldH	40	154	17.7
A0A2N0XCP3	GldN	36	312	35.6
A0A2N0XG70	GldD	28	185	21.8
A0A2N0XAR9	SprF	59	316	35.3
A0A2N0XB76	SprA	50	2346	263.5
A0A2N0XCE5	SprT	57	260	29.9

PMSZPI (Khare et al., 2020, 2022a). These motility proteins were predicted by the T9GPred web tool as well (Table 2). All of these identified T9SS associated proteins are essential for gliding motility, protein secretion and surface localization of cell surface motility adhesins in *F. johnsoniae* (Braun and McBride, 2005; Rhodes et al., 2011; Shrivastava et al., 2013) .

3.3.1. *Structure of colonies varies under spreading and non-spreading conditions*

Motile members of *Bacteroidota* form colonies with spreading edges that are hallmarks of gliding motility. PMSZPI was shown to harbor all essential gliding motility proteins (Table 3) and demonstrated spreading colony formation (Fig.1). The colony spreading is influenced by the concentrations of nutrients and agar available in the growth medium (McBride, 2019). The effect of agar concentration on colony spreading was observed by inoculating 10 µl ($OD_{600\ nm}$ 1.0) of PMSZPI cells on 1/10 LB agar media containing different concentrations of agar ranging from 0.35 %−1.5 % and incubating at 30 °C for 24 h The LB concentration was maintained at 1/10 as the previous studies on various *Bacteroidota* members had shown induction of colony spreading with decreased nutrient concentration (Khare et al., 2022a; Nakane et al., 2021). The colony on 1/10 LB 0.35 % agar plate exhibited the highest spreading with a mean colony diameter of ~4 cm whereas the least spreading of the colony was observed on 1/10 LB 1.5 % agar with a mean colony diameter of ~0.7 cm within 24 h of incubation (Fig. 1A). The culture grew to form unstructured thin film colony on 1/10 LB 0.35 % agar whereas the colony expansion appeared to be inhibited on 1/10 LB 1.5 % agar (Fig. 1Bi). Gliding and other forms of bacterial motility were found to be more pronounced when the cells were grown on medium containing low agar concentrations (Burchard, 1981). The irregular notched outline of the colony on 1/10 LB 0.35 % was visible in contrast to the colony formed on 1/10 LB 1.5 % agar that showed a regular outline (Fig. 1Bi). The corresponding stereomicroscopic examination of the microcolony on 1/10 LB 0.35 % agar showed branched edges linked to cell migration emanating radially from the site of inoculation (Fig. 1Bii). A closer inspection revealed a halo zone surrounding the terraced edges of the colony (Fig. 1Bii, inset) which could be due to the secretion of extracellular polymeric matrix (EPM). The detailed structure analysis of the spreading colony of *F. johnsoniae* suggested that the cells glided on the agar surface with the help of adhesins like SprB together with the secretion of EPM that preceded the migration of the cells (Sato et al., 2021a).

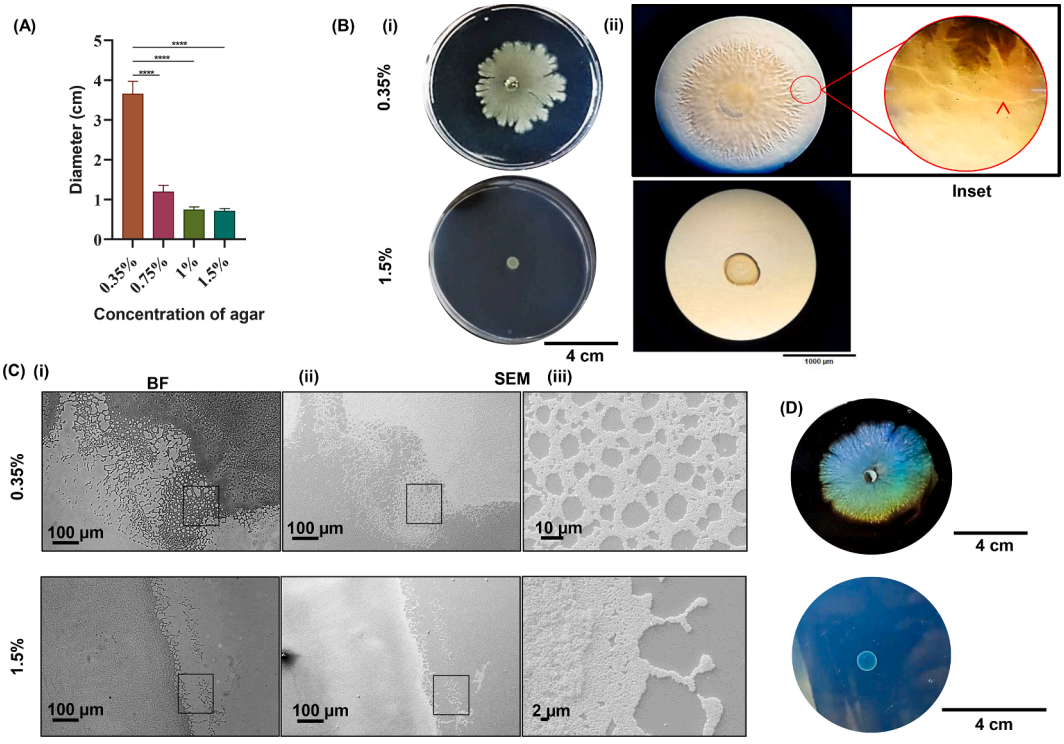

Fig. 1. Physiological characterization of spreading and non-spreading colonies of PMSZPI. (A) Average colony size (diameter) of microcolonies as a function of agar concentration ranging from 0.35 % to 1.5 % in nutrient depleted (1/10 LB) media. A decrease in colony size with increasing agar concentration was observed. Data represented in the graph are mean values ± SEM ($n = 3$). ANOVA was performed for the statistical analysis: *$p < 0.05$; **$p < 0.01$; ***$p < 0.001$;****$p < 0.0001$. (B) Morphology of the spreading and non-spreading colonies (i) that were imaged with stereomicroscope (ii). The spreading colony (on 0.35 % agar) demonstrated serrated edges and appeared to secrete a halo layer (inset) suggestive of an extracellular polymeric matrix (EPM) (indicated with a red arrow). A uniform, small circular colony was observed on hard agar (1.5 %). (C) Imaging of edges of spreading and non-spreading colonies. Bright field (BF) (i) and (ii) SEM imaging of colony edges were done. Cells on the edges of the spreading colony were periodically arranged with air spaces in contrast to the tightly packed cellular organization on the edges of the non-spreading colony. The black squares in BF and SEM images (i) and (ii) were correlated and further imaged with SEM at higher magnification (iii). (D) Structural coloration or iridescence of spreading and non-spreading colonies. The representative images are of biological triplicates.

On visualization with bright field microscopy, the serrated irregular periphery of spreading colonies on 1/10 LB 0.35 % agar revealed an extensive 'mesh' like arrangement of the cells whereas the non-spreading colonies on 1/10 LB 1.5 % agar exhibited very limited branched cell clusters at the tip of the leading edges (Fig. 1 Ci). To examine the ultrastructure of the edges in spreading and non-spreading colonies, a correlation of the regions visualized with BF microscopy was done with CLSEM (Fig. 1Cii) and such correlated areas were further magnified by SEM (Fig. 1Ciii). Consequently, highly resolved and magnified correlated areas of the colony edges with SEM revealed the remarkable self-assembly of cell clusters in the form of regular lattices with air spaces interspersed within the cell clusters in spreading colonies in contrast to non-spreading colonies that exhibited tightly packed cells at the colony edges (Fig. 1Ciii). The spreading colonies exhibited bright iridescence or coloration on illumination with white light that was not visualized with non-spreading colonies (Fig. 1D). Our previous studies and results from other investigations had suggested that gliding motility resulted in spreading colonies that were strongly linked to structural coloration or iridescence in the gliding bacteria of *Bacteroidota* phylum (Johansen et al., 2018; Khare et al., 2022a). The gliding motility facilitated the self-organization of cells into regular lattices that reflected light and gave rise to angle-dependent colouration (Johansen et al., 2018; Khare et al., 2022a; Kientz et al., 2012).

3.4. Single and collective cellular movement in the spreading colony

Following time lapse microscopy, attempts were made to track the motility of individual cells in the microcolony on soft agar (Fig. 2A). We captured images at 25 frames per second and the frames were then processed using ImageJ software. A manual tracking plugin was used to trace the tracks of individual cells gliding on soft agar. Time-lapse microscopy images were then processed using ImageJ software by tracking the cell centroid and cell displacement to calculate the mean cell speed. The cells appeared to glide on soft agar coming in contact with the fresh area of the agar substrate (Supplementary Movie 1). It was seen that any two colliding cells were not crawling over each other indicating the monolayer pattern of the cells. Also, these colliding cells appeared to stick together enhancing their speeds (Supplementary Movie 1). The generated tracks (Fig. 2Bi) were converted to z-projections, which were then used to create kymographs for individual cells (Fig. 2Bii). The motile cells frequently switched their travel directions, leaving zigzag tracks indicating cell movement over time in each frame represented by the kymographs, while the kymographs of non-motile cells were observed to be straight lines suggesting no cell displacement over time. The generated kymographs were manually traced using the line segment tool to calculate the mean cell speed of cells using the velocity tool plugin. The median speed of individual PMSZPI cells (no. of microscopic fields = 9) as derived from the kymographs is ~0.66 μm s^{-1} (Fig. 2Biii).

Subsequently, temporal and spatial resolution imaging was undertaken to detail the processes that facilitate spreading in the colonies. Cell suspensions of 1 μl were spotted on glass slides with either 1/10 LB 0.35 % agar or 1/10 LB 1.5 % agar. Radial colony expansion was observed and the colony edges started growing after 3 h of spotting of the culture on 1/10 LB 0.35 % agar. The movement of the colony edges was tracked by time-lapse microscopy. Rapid migration of the leading edges of the colony was suggestive of cooperative cell movement on soft agar that quickly populated the coverage area under observation and led to colony expansion (Fig. 2 Ci, ii). In contrast, there was hardly any movement of the colony edges observed for cultures spotted on hard agar. The colony edges appeared to remain static (Fig. 2 Ci, ii). Further, the z-stack high magnification BF images on soft agar exhibited tight, uniform packing of the cells at the centre whereas the cells at the edges were found to be arranged in layers in the direction of spreading (Fig. 2Di, ii). The three-dimensional (3D) structure of the colony extending from the base to the top of the microcolony on soft agar exhibited the invasion of the PMSZPI cells into the soft agar substrate possibly due to physical movement via

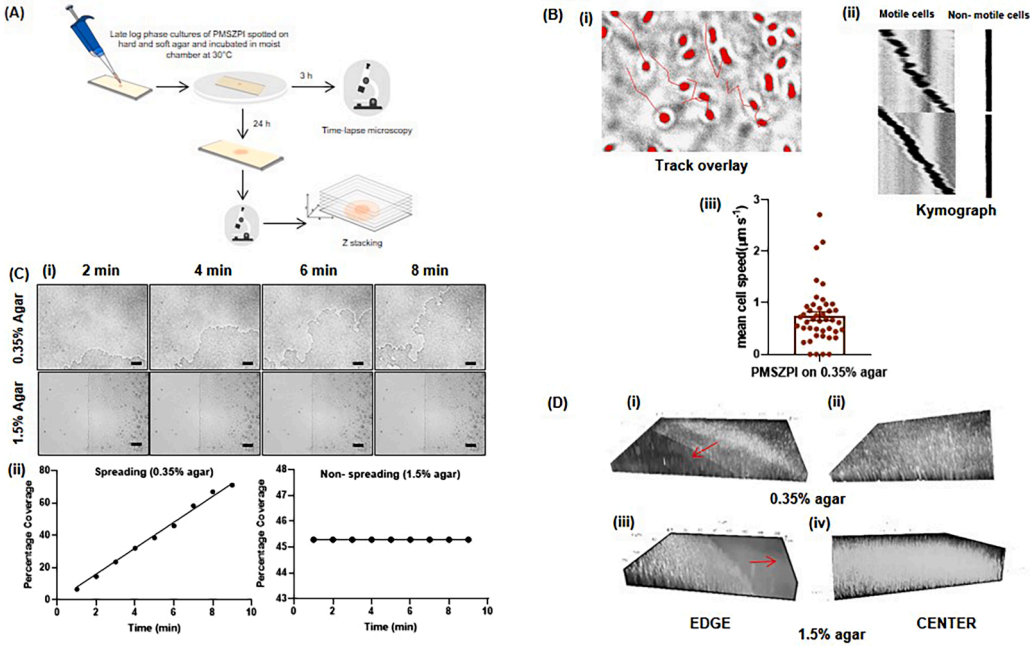

Fig. 2. Evaluation of the individual and collective cell motility in PMSZPI microcolonies on soft and hard agar. (A) Schematic representation of the experimental set-up employed for time lapse microscopy analysis of progressive edges of PMSZPI cells on hard and soft agar. (Designed using Inkscape v1.3.2) (B) Motility behavior of individual cells in spreading and non-spreading colonies. (i) Manual tracking of PMSZPI cells on soft agar following 3 h of incubation at 30°C using ImageJ. (ii) Kymographs representing the motile and non-motile cells of PMSZPI. (iii) The speed (μm s^{-1}) of individual cells. It was evaluated from nine microscopic fields using the velocity tool on ImageJ. Data represented in the dot plot are speeds ± the standard error mean. (C) Time-lapse imaging of progressive edges of PMSZPI microcolonies on 0.35 % or 1.5 % agar after 3 h of incubation at 30°C (i) and their corresponding coverage (percentage) area on agar surfaces as a function of time (ii). (D) Z-stack microscopic images of edges and centres of spreading (11 and 15 slices respectively) (i, ii) and non-spreading colonies (15 and 74 slices respectively) (iii, iv). The red arrow indicates the direction of the progressing edge of the microcolonies. The representative images are of biological triplicates.

gliding motility (Fig 2Di, ii). The cell density and the thickness of the colony at the centre and the edges on hard agar were higher as compared to that grown on soft agar and the cells at the edges did not show a layered arrangement of the cells (Table S2 and Fig. 2Diii, iv). The cell viability across the microcolonies under both spreading and non-spreading conditions was found to be intact as assessed by staining using Syto9 and propidium iodide (PI) (Fig. S3).

3.5. Differential gene expression analysis of PMSZPI cells under spreading and non-spreading conditions

RNA-Seq analysis was used to explore the differentially expressed genes (DEGs) among the spreading and non-spreading colonies of PMSZPI and to examine whether there is any linkage of the colony spreading phenotype observed under soft substrate conditions with the expression of T9SS-gliding motility-associated genes. The RNA extracted from colonies of *Chryseobacterium* sp. PMSZPI grown under spreading and non-spreading conditions were sequenced using the Illumina technology. The schematic representation of the methodology followed for RNA sequencing is provided in Fig. 3A. The average mapped reads for spreading and non-spreading colonies were 15.43 million and 16.9 million respectively. The total mapped RNA-Seq reads of 6 samples were ~70 % of the trimmed raw reads (Fig. S4). Principal component analysis performed to assess the transcriptomic similarity among the biological replicates in each case (spreading and non-spreading) exhibited the anticipated clustering of the triplicates (Fig. 3B). A higher biological variability among the replicates was observed that could be attributed to uncontrolled environmental conditions. However, there was a clear separation between spreading and non-spreading samples indicating that the gene expression pattern is indeed influenced by the agar substrate concentration (0.35 % agar or 1.5 % agar). DEGs under spreading and non-spreading conditions were identified with the value of $\log_2$ (fold Change) $>$ 1 and adjusted P-value $<$ 0.05. A total of 353 upregulated and 198 downregulated genes were identified using DESeq analysis. The gene expression of 6 samples was also presented as a heatmap and dendrogram (Figs. 3C, D). The differentially expressed genes were grouped based on the gene functions (Fig. 3E) in biological, molecular and other processes. The mainly upregulated functions included the metabolic pathways and cell structure synthesis. However, molecular processes associated with translation, DNA regulation and transcription were downregulated (Fig. 3E).

3.6. Upregulation of core T9SS-associated gliding motility genes under spreading conditions

Among the 15 core essential genes for motility and T9SS, only two of the genes *gldM* and *gld N* were upregulated by 1.47 and 2.53 $\log_2$(fold change) respectively in the RNA Seq analysis. The low-abundance transcripts of T9SS-associated gliding motility genes might have escaped detection in RNA-seq, therefore real-time PCR was undertaken for a better representation of gene expression. The qPCR performed to assess the expression of all the core T9SS-gliding genes confirmed the significant upregulation of *gldK, gldL, gldM, gldN, gldB, gldD, gldH, gldJ, sprE and sprT* in spreading colonies (Fig. 4). These results confirmed that the spreading phenotype observed in *Chryseobacterium* sp. strain PMSZPI grown on soft agar indeed resulted from upregulation of gliding motility genes in the organism.

3.7. Spreading affects the expression of T9SS-associated secretion, lipopolysaccharide, peptidoglycan and amino acid synthesis

In addition to upregulated levels of core gliding motility genes, there is an increase in T9SS-associated secretory proteins (Table 4). T9SS-mediated secreted proteins have signature C-terminal domains (CTD) (Kulkarni et al., 2017; McBride, 2019). These CTDs are unique and have varying motif sequences based on which they are classified as type A, B

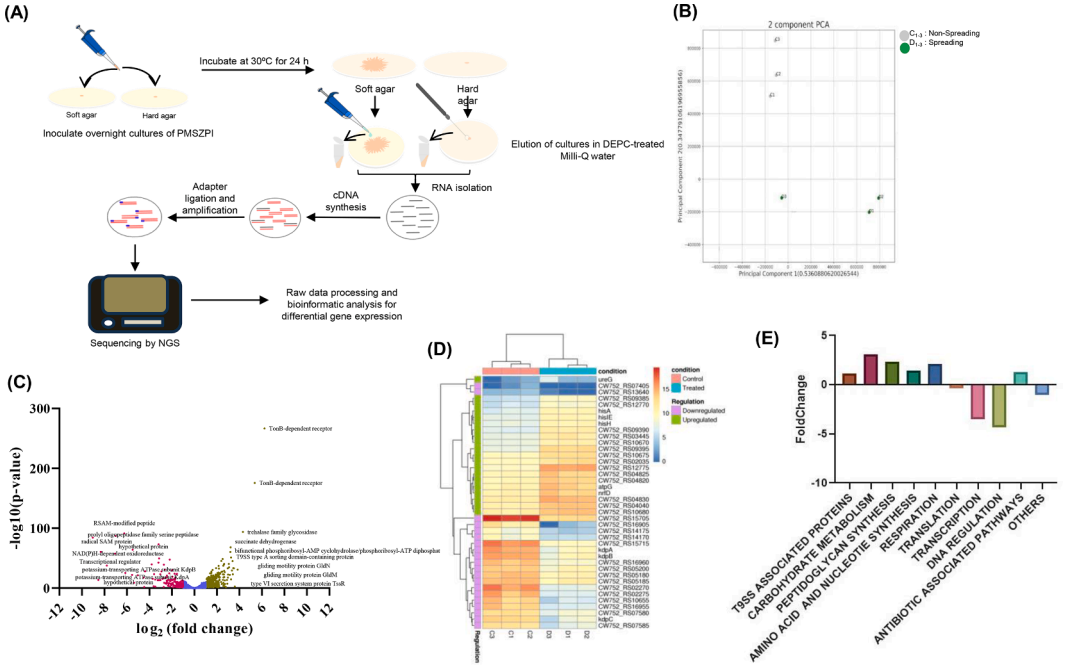

Fig. 3. RNA Sequencing of differential gene expression of PMSZPI in spreading conditions compared to non-spreading conditions. (A) Schematic representation of experimental setup involved in RNA sequencing of PMSZPI cells from hard and soft agar. (Designed using Inkscape v1.3.2) (B) Qualitative information of the samples of RNA Seq data indicating the PCA clustering of the triplicate samples of each condition of spreading and non-spreading. (C) Differentially expressed genes (DEGs) were identified in the spreading as compared to the non-spreading colonies of PMSZPI. (C) Expression heatmap of DEGs by hierarchical clustering of top 20 upregulated and downregulated genes. (D) Volcano plot of DEGs with 352 upregulated genes indicated in red dots and 198 downregulated genes indicated in blue dots. The blue dots indicate no significant differential gene expression. (E) DEGs grouping based on biological process, cellular component and molecular function with $\log_2$(fold change).

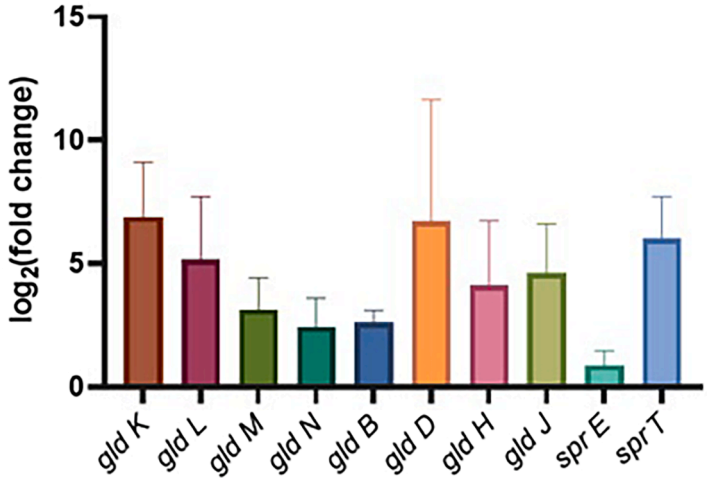

Fig. 4. RT-qPCR of the core gliding and T9SS genes. Upregulation of core gliding genes. Significant expression of core gliding genes, *gldK, gldL, gldM, gldN, sprE, sprT, gldB, gldD, gldH, and gldJ* was observed in the spreading PMSZPI colonies. Data represented in the graph are mean values ± the standard error mean.

Table 4
Differential gene expression of gliding motility and T9SS associated genes under spreading vs non-spreading conditions.

Gene ID	Product	log_2(fold change)
CW752_RS04040	Secretion protein :DUF5074 domain-containing protein	3.255661746
CW752_RS13155	gliding motility protein GldN	2.536403291
CW752_RS12070	T9SS type A sorting domain-containing protein	2.156200765
CW752_RS04070	hypothetical protein	1.84571449
CW752_RS08685	T9SS type A sorting domain-containing protein	1.71501959
CW752_RS04025	T9SS type A sorting domain-containing protein	1.676150197
CW752_RS00530	hypothetical protein	1.541547806
CW752_RS13160	gliding motility protein GldM	1.478483924
CW752_RS11950	T9SS type A sorting domain-containing protein	1.448824141
CW752_RS04020	T9SS type A sorting domain-containing protein	1.350942817
CW752_RS04315	T9SS type B sorting domain-containing protein	1.269023325
CW752_RS06300	T9SS type A sorting domain-containing protein	1.23607984
CW752_RS04310	hypothetical protein	1.216725328
CW752_RS05140	hypothetical protein	1.165597439
CW752_RS08615	T9SS type A sorting domain-containing protein	1.162238497
CW752_RS11045	T9SS type A sorting domain-containing protein	1.086901093
CW752_RS00545	T9SS type A sorting domain-containing protein	1.072457256
CW752_RS10425	PorT family protein	1.054741977
CW752_RS01620	T9SS type A sorting domain-containing protein	1.036849098
CW752_RS01670	PorT family protein	1.008053121
CW752_RS02170	T9SS type A sorting domain-containing protein	−1.242747965
CW752_RS04235	hypothetical protein	−1.24992325
CW752_RS10440	T9SS type A sorting domain-containing protein	−1.302685631

and C (Kulkarni et al., 2017; Sato et al., 2013; McBride 2019). In the omics data obtained in our experimental conditions, we observed a significant upregulation of multiple type A sorted T9SS secretory proteins (Table 4).

Increased expression of multiple enzymes that are part of the metabolism of various carbohydrates, amino acids and nucleotides was observed. Trehalases like glycosidase and other enzymes of the tricarboxylic acid cycle (TCA) which are part of carbohydrate metabolism were upregulated (Table 5). Certain enzymes that are involved in the synthesis of various amino acids like methionine, threonine, isoleucine, leucine, histidine, and arginine were upregulated (Table 5). On the contrary, cysteine synthase A and serine O- acetyltransferase which are involved in cysteine synthesis were significantly downregulated. Multiple protein subunits involved in oxidative phosphorylation are also upregulated. Apart from these multiple membrane-associated TonB receptors, enhanced expression of SusA, SusB, SusD/RagA, RagB, and other effluxes was observed (Table 5). A significant upregulation of genes like *murG, murC, murD, mraY, wecB, ftsA, ftsW, mraZ,* and *ftsZ* was observed under spreading conditions. Various oxidoreductases that are part of the electron transport chain and Kdp-potassium efflux pumps were upregulated. The expression of genes involved in the dynamics of nucleotide and protein synthesis pathways were observed to be downregulated, including certain transcriptional regulatory genes, GreAB, transposons and tRNAs. Contrarily, multiple ribosomal subunits and RNA ligases were upregulated (Table 5).

4. Discussion

The self-motile bacteria have the advantage of seeking out favourable growth conditions that allow them to acquire larger individual shares of environmental resources and confer fitness advantage. *Bacteroidota* is a dominant phylum among the soil microbiota. Apart from other supportive features, the phylum-specific Type IX Secretion System (T9SS) and its associated gliding motility provides the members of *Bacteroidota* a strong benefit over other competitive species in the soil environment that aids their colonization, adaptation and survival (Larsbrink and McKee, 2020). The findings presented here reveal the dynamic gliding motility responses of a *Bacteroidota* bacterium, *Chryseobacterium* PMSZPI, to the varied surface conditions. By focusing on strain PMSZPI, we contribute to a broader understanding of gliding motility across the *Bacteroidota* phylum, highlighting its adaptive significance in nutrient-deficient conditions typical of metal enriched areas like the one (uranium ore deposit) mentioned in this study. Through a multifaceted approach encompassing genomic and proteomic analysis, phenotypic characterization, microscopic examination and transcriptomic profiling, this study offers valuable insights into the attributes of gliding motility on varied environmental surfaces in this soil bacterium.

The phylogenetic analysis in this study shed light on the evolutionary relationships between gliding motility and the T9SS genes among the *Bacteroidota* members. The close phylogenetic affinity observed between the *Chryseobacterium* sp. PMSZPI and *Riemerella anatipestifer* underscores

Table 5
Differential expression for genes involved in metabolic, molecular and other pathways under spreading vs non-spreading conditions of PMSZPI.

Gene ID	Product	Log_2 (fold change)
Carbohydrate Metabolism		
CW752_RS09390	trehalase family glycosidase	4.309502594
CW752_RS10670	succinate dehydrogenase	3.221211385
CW752_RS08290	succinate dehydrogenase/fumarate reductase iron-sulfur subunit	2.577209794
Peptidoglycan Synthesis		
CW752_RS06060	undecaprenyldiphospho-muramoylpentapeptide beta-N-acetylglucosaminyltransferase	2.654884403
CW752_RS06055	UDP-N-acetylmuramate–l-alanine ligase	2.305275343
CW752_RS06070	UDP-N-acetylmuramoyl-l-alanine–d-glutamate ligase	2.253622193
CW752_RS06075	phospho-N-acetylmuramoyl-pentapeptide-transferase	2.190698568
Amino acid and nucleotide Synthesis		
CW752_RS03445	homoserine dehydrogenase	3.840322627
CW752_RS01470	1-(5-phosphoribosyl)−5-[(5-phosphoribosylamino)methylideneamino] imidazole-4- carboxamide isomerase	3.460264623
CW752_RS01570	3-isopropylmalate dehydratase large subunit	2.183070421
CW752_RS01480	bifunctional phosphoribosyl-AMP cyclohydrolase/phosphoribosyl-ATP diphosphatase HisIE	3.198298381
CW752_RS01465	imidazole glycerol phosphate synthase subunit HidH	2.963853734
CW752_RS01460	bifunctional histidinol-phosphatase/ imidazoleglycerol-phosphate dehydratase HisB	2.695009641
CW752_RS01475	imidazole glycerol phosphate synthase subunit HidF	2.616028169
CW752_RS12950	asparagine synthase B	2.573916791
CW752_RS01565	2-isopropylmalate synthase	2.488664081
CW752_RS05825	adenylosuccinate synthetase	−2.322152484
CW752_RS05265	cysteine synthase A	−2.813980104
CW752_RS03445	homoserine dehydrogenase	3.840322627
CW752_RS05270	serine O-acetyltransferase	−2.584478142
Respiration and electron transport chain		
CW752_RS04830	quinol:cytochrome C oxidoreductase	3.514025176
CW752_RS04825	c-type cytochrome	3.422837743
CW752_RS02235	ATP synthase F1 subunit gamma	3.258756654
CW752_RS02240	F0F1 ATP synthase subunit alpha	2.539669086
CW752_RS16520	NADH-quinone oxidoreductase subunit N	2.239551674
CW752_RS14705	cytochrome c oxidase accessory protein CcoG	2.231590735
CW752_RS16535	NADH-quinone oxidoreductase subunit NuoK	2.170536016
CW752_RS16555	NADH-quinone oxidoreductase subunit NuoH	2.113689044
CW752_RS16530	NADH-quinone oxidoreductase subunit L	2.040716069
CW752_RS11540	NAD(P)H-dependent oxidoreductase	−2.238565691
Translation		
CW752_RS01485	2′−5′ RNA ligase	2.645709871
CW752_RS03720	30S ribosomal protein S8	2.175872542
CW752_RS03710	50S ribosomal protein L18	2.144793546
CW752_RS03715	50S ribosomal protein L6	2.142349432
CW752_RS03725	30S ribosomal protein S14	2.140192653
CW752_RS08600	50S ribosomal protein L7/L12	2.114887529
CW752_RS13615	tRNA-Asn	−2.045669674
CW752_RS13610	tRNA-Glu	−2.135828831
CW752_RS16765	tRNA-Cys	−2.352508902
CW752_RS13620	tRNA-Ile	−2.732144618
CW752_RS13640	tRNA-His	−3.623817606
CW752_RS07405	tRNA-Pro	−4.458265272
Transcription		
CW752_RS09075	Transcription elongation factor GreAB	−3.475199241
DNA Regulation		
CW752_RS10655	Transcriptional regulator	−7.78647063
CW752_RS05190	DNA-binding response regulator	−3.018950493
CW752_RS15750	Transposase	−2.288647597
Membrane proteins		
CW752_RS12775	TonB-dependent receptor	6.228470917
CW752_RS09395	TonB-dependent receptor	5.37079843
CW752_RS09385	MFS transporter	3.387001723
CW752_RS10680	porin	3.091591907
CW752_RS10675	anion permease	3.058389426
CW752_RS02295	outer membrane beta-barrel protein	2.640780285
CW752_RS02290	outer membrane beta-barrel protein	2.903076072
CW752_RS07660	RagB/SusD family nutrient uptake outer membrane	2.807208279
CW752_RS08040	biopolymer transporter ExbD	2.727687316
CW752_RS03845	TonB-dependent receptor	2.573301682
CW752_RS08915	SusD/RagB family nutrient-binding outer membrane lipoprotein	2.392330463
CW752_RS08905	SusD/RagB family nutrient-binding outer membrane lipoprotein	2.060913199
CW752_RS15715	TonB-dependent receptor	−6.992811865
CW752_RS07600	potassium-transporting ATPase subunit KdpA	−6.143169794
CW752_RS07595	potassium-transporting ATPase subunit KdpB	−5.53687064
CW752_RS07590	K(+)-transporting ATPase subunit C	−5.364339866
CW752_RS07585	outer membrane beta-barrel protein	−5.037415785
CW752_RS05180	efflux RND transporter permease subunit	−3.792358547
CW752_RS05185	efflux RND transporter periplasmic adaptor	−3.57700728
CW752_RS02280	signal recognition particle protein	−2.502311893
CW752_RS00970	DMT family transporter	−2.299062379
CW752_RS05815	hypothetical protein	−2.268661686
Antibiotic associated Pathways		
CW752_RS02035	thiopeptide-type bacteriocin biosynthesis	2.978509672
CW752_RS02040	lantibiotic dehydratase family protein	2.713078947
CW752_RS11945	hypothetical protein	2.515064382
CW752_RS12720	antibiotic biosynthesis monooxygenase	−3.194070385
Other Genes		
CW752_RS12770	thiol:disulfide interchange protein	2.987639633
CW752_RS09185	redoxin domain-containing protein	−2.591080862
CW752_RS05260	uroporphyrinogen-III C-methyltransferase	−2.377731618
CW752_RS00505	thioredoxin family protein	−2.021728649

the evolutionary conservation of these motility-associated genes within the Weeksellaceae family (Fig. S1). *Flavobacterium johnsoniae* has served as a model organism for decades amongst the *Bacteroidota* members for studying gliding motility over surfaces (McBride, 2019). PMSZPI harboured all core gliding motility genes that showed relatively lesser sequence similarity with those of *F. johnsoniae*. *Chryseobacterium* was demarcated from *Flavobacterium* as a novel genus of the family Flavobacteriaceae in 1994 (Vandamme et al. 1994). Phylogenetic relationships among representatives of the family Flavobacteriaceae based on comparisons of 16S rRNA sequence revealed the close relationship of *Chryseobacterium* with *Riemerella* (Bernardet et al., 2002). The computational tool T9GPred in combination with LC-MS/MS analysis established the presence of orthologs of vital gliding motility proteins in PMSZPI highlighting their conservation across diverse *Bacteroidota* members. Previously, out of thirteen gliding motility related proteins encoded in the draft genome of *Flavobacterium columnare*, only four proteins including GldN, GldM, and GldL could be detected by proteomic analysis using 2-D LC ESI-MS/MS. Detection of the reduced number of proteins was attributed to the planktonic growth of *F. columnare* in broth culture (Dumpala et al., 2010). However, proteomic analysis of the membrane fraction of *Chryseobacterium* PMSZPI grown similarly in broth culture identified all the core gliding motility components of *Bacteroidota*- GldK, GldL, GldM, GldN, GldB, GldD, GldH, GldJ, SprA, SprE and SprT (Table 3).

We observed how the semi-solid (soft) and solid (hard) agar surfaces influenced the cell motility of PMSZPI at individual and population levels. Agar hydrogel was used as a plausible model substrate for mimicking solid or semi-solid environmental surfaces that the bacteria colonize because of its convenient preparation, biological compatibility and superior water binding capacity (Harshey, 2003). Colony spreading of PMSZPI was found to be influenced by agar concentration and

nutrient supply. In nutrient-deficient (1/10 LB) soft (0.35 %) agar plates, the colonies exhibited increased spreading resulting in dendritic patterns at the edges in contrast to small, round colonies visualized on hard (1.5 %) agar plates (Fig. 1). Our results were in agreement with those obtained for *Chryseobacterium gleum* isolated from the nematode *Caenorhabditis elegans*-associated communities that showed an inability to glide on hard agar (Duckett et al., 2024) but in contrast to *F. johnsoniae* that demonstrated motility on hard agar (Sato et al., 2021b). The cell surface adhesin SprB-dependent gliding motility in *F. johnsoniae* was shown to be reduced on soft agar substrate resulting in smaller rounded microcolonies as compared to hard agar that showed larger microcolonies (Sato et al., 2021b). The absence of SprB adhesin in the reported genomes of *Chryseobacterium* genus including PMSZPI could explain the contrasting phenotypes of spreading colonies of *Flavobacterium* and *Chryseobacterium* on agar substrate.

On inspection of the PMSZPI cells in the microcolony on soft agar following 3 h incubation by time-lapse microscopy, the cells appeared to oscillate back and forth from the point of their location (Fig. 2, Supplementary Movie 1). However, the cumulative shift of each cell when calculated and represented via kymographs indeed confirmed the movement of the cells by gliding. The speed of the PMSZPI cells (0.6 μm s^{-1}) on soft agar was found to be far less than that of *F. johnsoniae* cells that moved with a speed of ~ 10 μm s^{-1} on hard agar (Braun et al., 2005) and 2 μm s^{-1} on wet glass surfaces (Mark and Zhu, 2013). Individual cells of PMSZPI moved by gliding motility and aggregated to form spreading colonies. Such colonies arising from the collective or social movement of the cells have been shown to form biofilms in *F. johnsoniae* (Li et al., 2021; Sato et al., 2022). The closely packed and periodically arranged cells in these biofilms exhibited angle-dependent structural coloration or iridescence (Johansen et al., 2018; Kientz et al., 2016; Kientz *et.al.,* 2018) that was also observed with PMSZPI colonies with spreading edges (Fig. 1D). Cellular communication within the cells is mediated through mechanisms such as quorum sensing and chemotaxis. This enabled motile cells to form swarm colonies or fruiting bodies in various organisms (Branda et al., 2001; Zusman et al., 2007). However, to date, there are no reports of coordinated communication among *Bacteroidota* during spreading or gliding colony formation. The intricate microscopic organization observed in spreading colonies of PMSZPI suggested the existence of an unknown mechanism that controlled colony expansion based on environmental cues.

Transcriptomic analysis revealed the gene expression dynamics in PMSZPI cells underlying gliding motility, indicating the upregulation of core T9SS and gliding motility genes under spreading conditions on soft agar. This is in contrast to the findings in *F. columnare* wherein the highest expression of the gliding motility genes like *gldG, gldH, gldL and sprE* was observed under non-spreading conditions (Penttinen et al., 2018). Although the nutrient levels were found to regulate the expression of gliding motility genes in *F. columnare* to some extent, no clear correlation could be established between more active spreading/gliding and the expression of gliding motility genes (Penttinen et al., 2018).

Our study sheds light on the metabolic dynamics behind the active spreading of *Bacteroidota*, which is an area lacking comprehensive investigation in the literature. Other than gliding motility genes, we observed significant upregulation of genes associated with various metabolic pathways, including the tricarboxylic acid (TCA) cycle, oxidative phosphorylation, peptidoglycan synthesis, amino acid synthesis and cell division-related processes, under spreading conditions. The trehalases emerged as highly upregulated genes among other glycosidase genes, accompanied by an increase in Sus-TonB transmembrane transporters (Table 5). Sus transmembrane transporters and various glycosidases are integral components of PULs in *Bacteroidota* (McKee et al., 2021) and their gene expression facilitates the utilization of complex polysaccharides in the microbial environment. There are also reports suggesting the secretion of these glycosidases through the T9SS (Hehemann et al., 2012; Larsbrink et al., 2016).The *Bacteroidota* members have efficient sensing mechanisms to detect complex carbon structures, leading to the activation of polysaccharide utilization loci (PULs) or other non-canonical PULs to secrete enzymes specifically targeting polysaccharides for utilization. As bacteria encounter abundant resources in their surroundings, genes involved in metabolization undergo upregulation. Moreover, under conditions conducive to spreading, such as low agar concentration, higher water content facilitates nutrient diffusion, potentially aiding in nutrient absorption and promoting growth and motility, contrasting with conditions on hard substrates. This phenomenon of agar sensing and nutrient acquisition based on substrate properties has been observed in swarming organisms (Partridge and Harshey, 2013). An active upregulation of amino acid synthesis, except for cysteine synthesis was observed in our studies. However, it is essential to acknowledge that the data obtained from studies on gliding-spreading colonies may be biased due to their multicellular nature, which enables the division of labour across different colony interfaces (Li et al., 2021).

The gliding machinery in motile cells is hypothesized to be powered by the proton motive force (Vincent et al., 2022) unlike other motility types that rely on ATP. Consistent with this, our transcriptome data revealed increased expression of subunits electron transport chain, which is the main source of the proton motive force, thus providing energy for the motile cells. Universal stress proteins respond to various stresses such as osmotic stress, temperature fluctuations, and nutrient availability. In *E. coli*, the signalling of universal stress proteins is regulated by the action of the RpoS-sigma 70 factor, which dictates or regulates the levels of the universal protein UpsA. In some organisms, such as those employing quorum sensing, the expression of universal stress proteins is regulated accordingly (Kim et al., 2012; Nachin et al., 2005). In spreading colonies of PMSZPI, there is evident downregulation of both Sigma 70 and UpsA (Table 5) suggesting that gliding bacteria could apparently benefit from their motility and scavenging ability, unlike sessile non-spreading cells, that experience higher stress levels due to their sedentary nature and lower nutrient acquisition ability on hard agar.

RNA sequencing of various strains and their colony types could facilitate our understanding of gene expression under different substrate conditions that will help to gain a broad perspective on various factors that are associated with gliding motility. However, regulation of various pathways of *Bacteroidota* gliding motility still remains an enigma.

5. Conclusion

Gliding motility represents a social behaviour that contributes to organismal adaptation. Our findings for the first time provide valuable insights into various attributes of gliding motility on hard and soft substrates in the environmental strain, *Chryseobacterium* sp. PMSZPI, isolated from uranium/heavy metal enriched area. The collective cellular movement in PMSZPI owing to gliding motility on semi-solid/soft surfaces could have possibly played an important role in nutrient acquisition and colonization. The environmental surfaces to a great extent contribute to the regulation of motility related genes. There is little information on the correlation of bacterial gliding motility with metals. The analysis of the role of gliding motility in the adaptation of PMSZPI in metal-enriched environment through the utilization of genetic manipulation techniques and physiological studies is in progress at our end that will help to enhance our understanding on the relationship of bacterial motility with environmental adaptation in diverse microbial communities.

Funding

This research did not receive any specific grant from funding agencies in the public, commercial, or not-for-profit sectors.

Declaration of competing interest

The authors declare that they have no known competing financial interests or personal relationships that could have appeared to influence the work reported in this paper.

Acknowledgements

The authors thank Pallavi Chandwadkar, MBD, BARC, Mumbai for correlative-SEM imaging of the samples.

Supplementary materials

Supplementary material associated with this article can be found, in the online version, at doi:10.1016/j.crmicr.2024.100309.

Data availability

No data was used for the research described in the article.

References

Bernardet, J.-F., Nakagawa, Y., Holmes, B., 2002. Proposed minimal standards for describing new taxa of the family *Flavobacteriaceae* and emended description of the family. Int. J. Syst. Evol. Microbiol. 52 (3), 1049–1070. https://doi.org/10.1099/00207713-52-3-1049.

Branda, S.S., González-Pastor, J.E., Ben-Yehuda, S., Losick, R., Kolter, R., 2001. Fruiting body formation by *Bacillus subtilis*. Proceed. Natl. Acad. Sci. 98 (20), 11621–11626. https://doi.org/10.1073/pnas.191384198.

Braun, T.F., Khubbar, M.K., Saffarini, D.A., McBride, M.J., 2005. *Flavobacterium johnsoniae* gliding motility genes identified by mariner mutagenesis. J. Bacteriol. 187 (20), 6943–6952. https://doi.org/10.1128/JB.187.20.6943-6952.2005.

Braun, T.F., McBride, M.J., 2005. *Flavobacterium johnsoniae* GldJ is a lipoprotein that is required for gliding motility. J. Bacteriol. 187 (8), 2628–2637. https://doi.org/10.1128/JB.187.8.2628-2637.2005.

Burchard, R.P., 1981. Gliding motility of prokaryotes: ultrastructure, physiology, and genetics. Annu. Rev. Microbiol. 35 (1), 497–529. https://doi.org/10.1146/annurev.mi.35.100181.002433.

Chang, L.-Y.E., Pate, J.L., Betzig, R.J., 1984. Isolation and characterization of nonspreading mutants of the gliding bacterium *Cytophaga johnsonae*. J. Bacteriol. 159. https://doi.org/10.1128/jb.159.1.26-35.1984, 159(1).

Duckett, M., Taylor, M.N., Bowman, C., Vega, N.M., 2024. Parallel evolution of alternate morphotypes of Chryseobacterium gleum during experimental evolution with *Caenorhabditis elegans*. FEMS Microbiol. Ecol. 100 (5), fiae039. https://doi.org/10.1093/femsec/fiae039.

Dumpala, P.R., Gülsoy, N., Lawrence, M.L., Karsi, A., 2010. Proteomic analysis of the fish pathogen *Flavobacterium columnare*. Proteom. Sci. 8 (1), 26. https://doi.org/10.1186/1477-5956-8-26.

Harshey, R.M., 2003. Bacterial motility on a surface: many ways to a common goal. Annu. Rev. Microbiol. 57 (1), 249–273. https://doi.org/10.1146/annurev.micro.57.030502.091014.

Hehemann, J.-H., Correc, G., Thomas, F., Bernard, T., Barbeyron, T., Jam, M., Helbert, W., Michel, G., Czjzek, M., 2012. Biochemical and structural characterization of the complex agarolytic enzyme system from the marine bacterium *Zobellia galactanivorans*. J. Biolog. Chem. 287 (36), 30571–30584. https://doi.org/10.1074/jbc.M112.377184.

Johansen, V.E., Catón, L., Hamidjaja, R., Oosterink, E., Wilts, B.D., Rasmussen, T.S., Sherlock, M.M., Ingham, C.J., Vignolini, S., 2018. Genetic manipulation of structural color in bacterial colonies. Proceed. Natl. Acad. Sci. 115 (11), 2652–2657. https://doi.org/10.1073/pnas.1716214115.

Khare, D., Chandwadkar, P., Acharya, C., 2022a. Gliding motility of a uranium-tolerant Bacteroidetes bacterium *Chryseobacterium sp.* strain PMSZPI: insights into the architecture of spreading colonies. Environ. Microbiol. Rep. 14 (3), 453–463. https://doi.org/10.1111/1758-2229.13034.

Khare, D., Chandwadkar, P., Acharya, C., 2022b. Structural analysis of gliding motility of a bacteroidetes bacterium by correlative light and scanning electron microscopy (CLSEM). Microsc. Microanaly. 28 (2), 515–521. https://doi.org/10.1017/S1431927622000095.

Khare, D., Kumar, R., Acharya, C., 2020. Genomic and functional insights into the adaptation and survival of *Chryseobacterium sp.* strain PMSZPI in uranium enriched environment. Ecotoxicol. Environ. Saf. 191, 110217. https://doi.org/10.1016/j.ecoenv.2020.110217.

Kientz, B., Luke, S., Vukusic, P., Péteri, R., Beaudry, C., Renault, T., Simon, D., Mignot, T., Rosenfeld, E., 2016. A unique self-organization of bacterial sub-communities creates iridescence in *Cellulophaga lytica* colony biofilms. Sci. Rep. 6, 19906. https://doi.org/10.1038/srep19906.

Kientz, B., Marié, P., & Rosenfeld, E. (2012). Effect of abiotic factors on the unique glitter-like iridescence of *Cellulophaga lytica*. In *FEMS Microbiol. Lett.,* 333(2), 101–108. https://doi.org/10.1111/j.1574-6968.2012.02614.x.

Kim, H., Goo, E., Kang, Y., Kim, J., Hwang, I., 2012. Regulation of universal stress protein genes by quorum sensing and RpoS in *Burkholderia glumae*. J. Bacteriol. 194 (5), 982–992. https://doi.org/10.1128/JB.06396-11.

Kulkarni, S.S., Zhu, Y., Brendel, C.J., McBride, M.J., 2017. Diverse C-terminal sequences involved in *Flavobacterium johnsoniae* protein secretion. J. Bacteriol. (12), 199. https://doi.org/10.1128/JB.00884-16.

Kumar, R., Nongkhlaw, M., Acharya, C., Joshi, S.R., 2013. Uranium (U)-tolerant bacterial diversity from U ore deposit of domiasiat in North-East India and its prospective utilisation in bioremediation. Microb. Environ. 28 (1), 33–41. https://doi.org/10.1264/jsme2.ME12074.

Larsbrink, J., McKee, L.S., 2020. Chapter Two - *Bacteroidetes* bacteria in the soil: glycan acquisition, enzyme secretion, and gliding motility. In: Gadd, G.M., Sariaslani, S. (Eds.), Chapter Two - *Bacteroidetes* bacteria in the soil: glycan acquisition, enzyme secretion, and gliding motility. Adv. Appl. Microbiol. 63–98. https://doi.org/10.1016/bs.aambs.2019.11.001.

Larsbrink, J., Zhu, Y., Kharade, S.S., Kwiatkowski, K.J., Eijsink, V.G.H., Koropatkin, N. M., McBride, M.J., Pope, P.B., 2016. A polysaccharide utilization locus from *Flavobacterium johnsoniae* enables conversion of recalcitrant chitin. Biotechnol. Biofuel. 9 (1), 260. https://doi.org/10.1186/s13068-016-0674-z.

Li, C., Hurley, A., Hu, W., Warrick, J.W., Lozano, G.L., Ayuso, J.M., Pan, W., Handelsman, J., Beebe, D.J., 2021. Social motility of biofilm-like microcolonies in a gliding bacterium. Nat. Commun. 12 (1), 5700. https://doi.org/10.1038/s41467-021-25408-7.

Mark, B.M., Zhu, Y., 2013. Gliding motility and por secretion system genes are widespread among members of the phylum *Bacteroidetes*. J. Bacteriol. 195 (2), 270–278. https://doi.org/10.1128/JB.01962-12.

McBride, M.J., 2019. Bacteroidetes gliding motility and the Type IX secretion system. Microbiol. Spectr. 7 (1), 363–374. https://doi.org/10.1128/microbiolspec.psib-0002-2018.

McKee, L.S., La Rosa, S.L., Westereng, B., Eijsink, V.G., Pope, P.B., Larsbrink, J, 2021. Polysaccharide degradation by the *Bacteroidetes*: mechanisms and nomenclature. Environ. Microbiol. Rep. 13 (5), 559–581. https://doi.org/10.1111/1758-2229.12980.

Nachin, L., Nannmark, U., Nyström, T., 2005. Differential roles of the universal stress proteins of *Escherichia coli* in oxidative stress resistance, adhesion, and motility. J. Bacteriol. 187 (18), 6265–6272. https://doi.org/10.1128/JB.187.18.6265-6272.2005.

Nakane, D., Odaka, S., Suzuki, K., Nishizaka, T., 2021. Large-Scale Vortices with Dynamic Rotation Emerged from Monolayer Collective Motion of Gliding *Flavobacteria*. J. Bacteriol. 203 (14), 10–1128. https://doi.org/10.1128/jb.00073-21.

Partridge, J.D., Harshey, R.M., 2013. Swarming: flexible roaming plans. J. Bacteriol. 195 (5), 909–918. https://doi.org/10.1128/JB.02063-12.

Penttinen, R., Hoikkala, V., Sundberg, L.R., 2018. Gliding motility and expression of motility-related genes in spreading and non-spreading colonies of *Flavobacterium columnare*. Front. Microbiol. (9), 285529. https://doi.org/10.3389/fmicb.2018.00525.

Rhodes, R.G., Pucker, H.G., McBride, M.J., 2011. Development and use of a gene deletion strategy for *Flavobacterium johnsoniae* to identify the redundant gliding motility genes remF, remG, remH, and remI. J. Bacteriol. 193 (10), 2418–2428. https://doi.org/10.1128/JB.00117-11.

Sahoo, A.K., Vivek-Ananth, R.P., Chivukula, N., Rajaram, S.V., Mohanraj, K., Khare, D., Acharya, C., & Samal, A. (2023). T9GPred: a comprehensive computational tool for the prediction of type 9 secretion system, Glid. Motil. Assoc. Secret. Prot., 8(37), 34091–34102. https://doi.org/10.1101/2023.03.31.535141.

Sato, K., Naito, M., Yukitake, H., Hirakawa, H., Shoji, M., McBride, M.J., Rhodes, R.G., Nakayama, K., 2010. A protein secretion system linked to bacteroidete gliding motility and pathogenesis. Proc. Natl. Acad. Sci. U.S.A. 107 (1), 276–281. https://doi.org/10.1073/pnas.0912010107.

Sato, K., Naya, M., Hatano, Y., Kondo, Y., Sato, M., Nagano, K., Chen, S., Naito, M., Sato, C., 2021a. Biofilm spreading by the adhesin-dependent gliding motility of *Flavobacterium johnsoniae*. 1. Internal structure of the biofilm. Int. J. Mol. Sci. 22 (4), 1894. https://doi.org/10.3390/ijms22041894.

Sato, K., Naya, M., Hatano, Y., Kondo, Y., Sato, M., Narita, Y., Nagano, K., Naito, M., Nakayama, K., Sato, C., 2021b. Colony spreading of the gliding bacterium *Flavobacterium johnsoniae* in the absence of the motility adhesin SprB. Sci. Rep. 11 (1), 967. https://doi.org/10.1038/s41598-020-79762-5.

Sato, K., Yukitake, H., Narita, Y., Shoji, M., Naito, M., Nakayama, K., 2013. Identification of *Porphyromonas gingivalis* proteins secreted by the Por secretion system. FEMS Microbiol. Lett. 338 (1), 68–76. https://doi.org/10.1111/1574-6968.12028.

Shrivastava, A., Johnston, J.J., Van Baaren, J.M., McBride, M.J., 2013. *Flavobacterium johnsoniae* GldK, GldL, GldM, and SprA are required for secretion of the cell surface gliding motility adhesins sprb and remA. J. Bacteriol. 195 (14), 3201–3212. https://doi.org/10.1128/JB.00333-13.

Singh, S.S., Mansuri, M.S., Naiyer, S., Kaur, D., Agrahari, M., Srinivasan, S., Jhingan, G. D., Bhattacharya, A., Bhattacharya, S., 2022. Multi-omics analysis to characterize molecular adaptation of *Entamoeba histolytica* during serum stress. Proteomics 22 (22), e2200148. https://doi.org/10.1002/pmic.202200148.

Tamura, K., Stecher, G., Kumar, S., 2021. MEGA11: molecular evolutionary genetics analysis version 11. Mol. Biol. Evol. 38 (7), 3022–3027. https://doi.org/10.1093/molbev/msab120.

Vincent, M.S., Hervada, C.C., Sebban-Kreuzer, C., Le Guenno, H., Chabalier, M., Kosta, A., Guerlesquin, F., Mignot, T., McBride, M.J., Cascales, E., Doan, T., 2022. Dynamic proton-dependent motors power type IX secretion and gliding motility in *Flavobacterium*. PLoS Biol. 20 (3). https://doi.org/10.1371/journal.pbio.3001443.

Zusman, D.R., Scott, A.E., Yang, Z., Kirby, J.R., 2007. Chemosensory pathways, motility and development in *Myxococcus xanthus*. Nat. Rev. Microbiol. 5 (11), 862–872. https://doi.org/10.1038/nrmicro1770.